How Dopamine Transporter Interacts with Dopamine: Insights from Molecular Modeling and Simulation

Xiaoqin Huang and Chang-Guo Zhan
Department of Pharmaceutical Sciences, College of Pharmacy, University of Kentucky, Lexington, Kentucky

ABSTRACT By performing homology modeling, molecular docking, and molecular dynamics simulations, we have developed three-dimensional (3D) structural models of both dopamine transporter and dopamine transporter-dopamine complex in the environment of lipid bilayer and solvent water. According to the simulated structure of dopamine transporter-dopamine complex, dopamine was orientated in a hydrophobic pocket at the midpoint of the membrane. The modeled 3D structures provide some detailed structural and mechanistic insights concerning how dopamine transporter (DAT) interacts with dopamine at atomic level, extending our mechanistic understanding of the dopamine reuptake with the help of Na^+ ions. The general features of the modeled 3D structures are consistent with available experimental data. Based on the modeled structures, our calculated binding free energy ($\Delta G_{bind} = -6.4$ kcal/mol) for dopamine binding with DAT is also reasonably close to the experimentally derived ΔG_{bind} value of -7.4 kcal/mol. Finally, a possible dopamine-entry pathway, which involves formation and breaking of the salt bridge between side chains of Arg^{85} and Asp^{476}, is proposed based on the results obtained from the modeling and molecular dynamics simulation. The new structural and mechanistic insights obtained from this computational study are expected to stimulate future, further biochemical and pharmacological studies on the detailed structures and mechanisms of DAT and other homologous transporters.

INTRODUCTION

Dopamine transporter (DAT) is an important protein for movement and Parkinsonism. Its native substrate, dopamine, is a vital neurotransmitter for locomotor control and reward systems, including those lost or deranged in Parkinson's disease (1). DAT is also the primary target of cocaine. Cocaine is the most reinforcing of all drugs of abuse (2,3,4). Through binding with DAT, cocaine blocks the clearance (reuptake) of dopamine from central nervous system synapses and thereby prolongs dopaminergic neurotransmission in brain areas associated with reward. There are millions of individuals worldwide addicted to cocaine. Such a public health crisis has carried a substantial burden to the society in the form of increasing medical expenses, lost earnings, and increased crimes associated with psychostimulant abuse. There is no available medication approved by Food and Drug Administration to be used against cocaine addiction (1,5). The disastrous medical and social consequences of cocaine addiction have made the development of an effective pharmacological treatment a high priority (6–13).

Physiologically, DAT spatially and temporally buffers released dopamine at synaptic cleft, terminating dopaminergic neurotransmission and reaccumulating dopamine into presynaptic neurons. The transporting process can be roughly modeled as involving several different DAT states: bound state for dopamine and ions; intracellular unloading state of dopamine and ions; and finally extracellularly facing state as an unloaded carrier (14,15). Pharmacological studies have shown that dopamine transporting by DAT is Na^+/Cl^--dependent. The overall stoichiometry is likely as dopamine/$Na^+/Cl^- = 1:2:1$ (16,17). Site-directed mutagenesis has been performed extensively on DAT to search for amino-acid residues responsible for the Na^+ action, dopamine binding, and their coupling with the actions of cocaine (18–29). However, molecular mechanisms for these actions have appeared as complex and bewildering. A knock-in mouse model with functional DAT has been developed and found to be insensitive to cocaine (5). Such progress is paving the way of fully understanding the structure-function relationships of DAT system. However, structural details about the interactions of DAT with dopamine, cocaine, and its analogs remain to be uncovered. These facts make highly desirable a study on how the DAT interacts with its substrate.

DAT is a member of the neurotransmitter sodium symporters (NSS) family, belonging to the ion-coupled secondary transporters superfamily (STS) (30–34). The STS is known as the largest superfamily of membrane proteins of transporters with more than 1000 identified members to date (30). Driven by a solute gradient, these proteins transport ions, drugs, neurotransmitters, and other hydrophilic solutes. Some typical members of this superfamily have been structurally characterized through x-ray crystallography and, therefore, their possible transporting mechanisms have been explored. For example, the Glycerol-3-phosphate transporter (GlpT) (Protein Data Bank, i.e., PDB entry of 1PW4 with a resolution of 3.3 Å) operates by a singly-binding site, alternating-access mechanism (30). Another typical example is the Lactose permease (LacY, PDB entry of 1PV7 with a resolution of 3.6 Å) as a representative of Lactose subfamily (31). Besides the protonated, inward-facing conformation of LacY with bound substrate, the outward-facing conformation open to the periplasmic side is considered to be required for the final

Submitted April 17, 2007, and accepted for publication July 26, 2007.

Address reprint requests to Chang-Guo Zhan, PhD, Tel.: 859-323-3943; E-mail: zhan@uky.edu.

Editor: Ron Elber.

0006-3495/07/11/3627/13 $2.00

doi: 10.1529/biophysj.107.110924

substrate transport across the membrane. Transporters in NSS family usually use sodium and chloride electrochemical gradients to catalyze the thermodynamically uphill movements for a series of substrates such as serotonin and dopamine (31,34). More recently, the x-ray crystal structure for a bacterial homolog ($LeuT_{Aa}$) of NSS from *Aquifex aeolicus* was determined in complex with substrate leucine and two sodium ions (PDB entry of 2A65 at 1.65 Å resolution) (34). This structure is viewed as an extracellularly faced state with the bound substrate. The possible substrate-entry pathway was proposed to be along transmembrane helices 1, 3, 6, and 8, starting from the extracellular end of these helices to the substrate-binding site. $LeuT_{Aa}$ shares similar topological features with GlpT and LacY, i.e., 12 transmembrane α-helices with intracellular localization of both N-terminal and C-terminal, and a large internal substrate-binding cavity on the midpoint of the membrane. However, $LeuT_{Aa}$ is quite different from GlpT and LacY (31,32,34). It bears a pseudo-twofold helix packing axis between helices 1–5 and helices 6–10, whereas GlpT and LacY have such a twofold axis between helices 1–6 and helices 7–12. The substrate-binding site in $LeuT_{Aa}$ is located among partially unwound transmembrane helices 1, 3, 6, and 8 with main-chain atoms and helix dipoles playing a key role in the binding of substrate and sodium ions (34). In GlpT and LacY, the hydrophilic cavity is among helices 1, 4, 5, 7, and 11. These three typical transporters with available x-ray crystal structures belong to different families of transporter proteins. Some molecular modeling has been performed on DAT, serotonin transporter (SERT), and noradrenalin transporter (NET) (35,36) by using Na^+/H^+ antiporter or LacY (31) as the template. Now it is obvious that these templates in previous modeling studies are not suitable for the homology modeling of any member of the NSS family. Hence, the predicted atomic interactions are not reliable. No experimental evidence has been reported to support the previously reported models from any kind of structural or biological studies. Therefore, the previously reported structural models of DAT, SERT, and NET are not good enough to be used for studying molecular interactions of psychotropic drugs with these transporters. With similar structural folding and physiological features as other NSS family members, $LeuT_{Aa}$ has been viewed as the most reasonable template to study the substrate binding and transporting mechanism for NSS transporters, especially for dopamine transporter and serotonin transporter (5).

In this work, a new three-dimensional (3D) structural model of DAT has been constructed through homology modeling based on the most reasonable template, i.e., the $LeuT_{Aa}$ structure (34), and refined by performing molecular dynamics (MD) simulations in the environment of lipid bilayer and solvent water. Based on the developed structural model of DAT, the substrate-binding mode has been determined through further molecular docking, MD simulations, and binding free energy calculations. Through MD simulations on both the DAT model without dopamine and the DAT-dopamine binding complex, a possible substrate-entry pathway has been proposed. The overall agreement between the computational results and available experimental data (16,21, 25,26,28) demonstrates important structural features of DAT and its binding with substrate, providing some valuable insight into the molecular mechanism for DAT modulating dopamine reuptake.

COMPUTATIONAL METHODS

Homology modeling and structural optimization of DAT in a physiological environment

To understand how dopamine binds with DAT and further explore the possible substrate-entry pathway, a 3D structural model of DAT was built based on the x-ray crystal structure of $LeuT_{Aa}$ (34) by using the Homology module from the InsightII software (Ver. 2000, Accelrys, San Diego, CA). The amino-acid sequence of human DAT was directly extracted from the NCBI databank (access No.: Q01959). The sequence alignment was generated by using ClusterW with the Blosum scoring function (37,38). The best alignment was selected according to both the alignment score and the reciprocal positions of the conserved residues among the NSS family. These include the NGGGF motif between transmembrane helix 1 and 2, and other residues around the Na^+ binding sites in DAT. The first 55 residues at the N-terminal and the last 32 residues at the C-terminal were omitted because of no corresponding homolog sequence in the template. A piece of 25 residues inside extracellular loop 2 was manually skipped under the template to get a better alignment at the conserved positions of Pro^{176} and Glu^{215} of DAT with the template and other members in the NSS family, including glycine transporter and serotonin transporter. The sequence identity reached 20.4% and the whole sequence homology became 42.0% for the final alignment (Fig. 1). The coordinates of the conserved regions were directly transformed from the template structure (i.e., the x-ray crystal structure of $LeuT_{Aa}$ (34)), while the nonequivalent residues were mutated from the template to the corresponding ones of DAT. The side chains of those nonconserved residues were relaxed by using the Homology module of InsightII to remove the possible steric overlap or hindrance with the neighboring conserved residues. The conformation of the inserted 25 residues inside extracellular loop 2 was searched from the internal database of InsightII software and the best fit was selected from the generated 10 candidates.

To simulate the actual physiological environment, the initial DAT model was inserted into a preequilibrated POPC lipid bilayer and then solvated by two layers of water molecules at each side of lipid bilayer. The POPC bilayer was generated by using the membrane plug-in of the VMD software (39) and the initial size of the membrane was expanded to be large enough to encompass the target protein. The geometry of POPC molecule was optimized by performing ab initio electronic structure calculation at the HF/6-31G* level using Gaussian-03 program (40). The HF/6-31G* calculation was also performed to determine the restrained electrostatic potential (RESP)-fitted charges for POPC molecules. The similar RESP-fitting calculations based on the first-principles electronic structure method were used in our previous computational studies of other protein-ligand systems and led to satisfactory binding structures (41–45). The relative orientation of DAT in the lipid bilayer was determined by referring the similar orientation of the $LeuT_{Aa}$ structure (34), i.e., transmembrane helix 12 in parallel with the normal of the membrane, the binding sites of two Na^+ placed at the midpoint of the membrane, and the two terminals (both N-terminal and C-terminal) intracellularly located. When inserting, any POPC molecule was removed if it had >50% of its nonhydrogen atoms within a distance of 2.5 Å to any nonhydrogen atoms of DAT. The solvent layers were added by using the LEaP module of AMBER8 program suite (46). The protein together with the lipid bilayer was solvated in a rectangular box of TIP3P water molecules (47) with a minimum solute wall distance of 10 Å. The redundant water molecules beyond

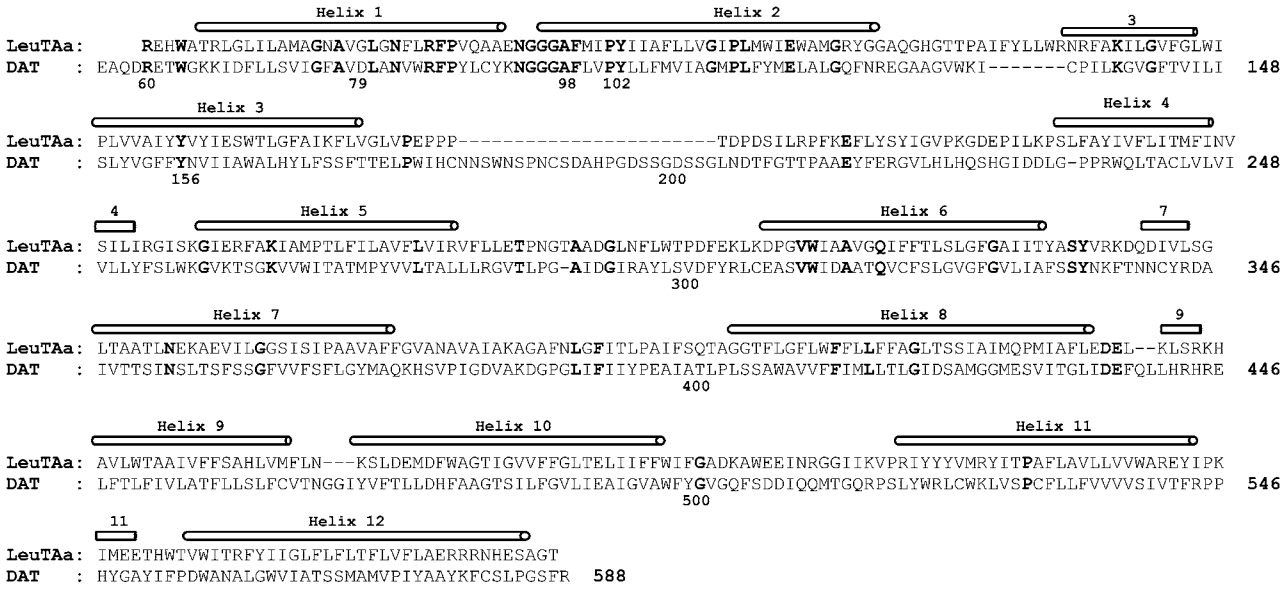

FIGURE 1 Sequence alignment of human DAT with the bacterial homolog of Na^+/Cl^--dependent neurotransmitter transporters ($LeuT_{Aa}$) by manual adjustment. Twelve helices are labeled above the sequence, and strictly conserved residues among the NSS family are shown in bold.

the *x*,*y* boundary of the membrane were cut off to match the size of lipid bilayer. Standard protonation states at physiological environment (pH ~7.4) were set to all ionizable residues of DAT, and the positions of protons were properly set on Nδ1 atom of His residues. Additional 4 Na^+ were added in the solvent as counterions to neutralize the whole system. The final system size was ~126 Å × 125 Å × 118 Å, composed of 154,114 atoms, including 351 POPC molecules and 32,390 water molecules.

After the whole system was set up, a series of energy minimizations (or geometric optimizations) were carried out by using the Sander module of AMBER8 program suite (46) with a nonbonded cutoff of 12 Å and a conjugate gradient energy-minimization method. The first 2000 steps of the energy minimization was done for the backbone of DAT while the side chains were fixed, and then the next 20,000 steps for the side-chain atoms with the backbone fixed. To get the solute (DAT) better solvated, the subsequent energy minimization and short-time MD simulations were performed on the environment (i.e., the lipid molecules, water molecules, and the counterions). After 50,000 steps of energy minimization on the environment, 80-ps MD simulations were performed on water molecules with NTV ensemble at $T = 300$ K. The environment was energy-minimized again for 20,000 steps followed by a 30-ps MD simulation on the lipid molecules. After these MD simulations, the environment and side chains of DAT were energy-minimized for 25,000 steps. Finally, the system was energy-minimized for 6000 steps for all atoms, and a convergence criterion of 0.001 kcal mol^{-1} $Å^{-1}$ was achieved.

Molecular docking and binding free energy calculation

Based on the structural model of DAT obtained in this study, the binding mode of dopamine with DAT was explored through molecular docking by using the AutoDock 3.0.5 program and the DOCK 5.4 program (48,49). The two different docking programs were used for the same system for the purpose of increasing the number of possible candidates of the binding complex. The atomic charges of the protonated dopamine were also determined as the RESP charges determined by using the standard RESP procedure implemented in the Antechamber module of the AMBER8 program (46) after the electronic structure and electrostatic potential calculations at the HF/6-31G*. During the AutoDock docking process, a conformational search was performed using the Solis and Wets local search method (50), and the Lamarckian genetic algorithm (48) was applied to deal with the DAT-dopamine interactions. Among a series of docking parameters, the grid size was set to be 60 × 60 × 60 and the grid space was the default value of 0.375 Å. Similar grid size was used in the DOCK 5.0 docking operation, and the protonated dopamine molecule was flexibly treated by using the anchor-and-grow algorithm (49). The possible binding site in DAT was first roughly defined as a similar site in $LeuT_{Aa}$ structure (34), i.e., the cavity around transmembrane helices 1, 3, 6, and 8. The binding site was then hunted by changing the center and the size of the docking grid. All the complex candidates were evaluated and ranked in terms of binding energy by using the standard energy score function implemented in the docking programs and the geometric matching quality.

As both the docking programs cannot consider the structural flexibility of the binding site during the docking process, further energy minimizations on those initially selected 20 complexes were performed in a similar way as described above, i.e., 10,000 steps with the fixed backbone of DAT, and then 15,000 steps or the convergence criteria 0.001 kcal mol^{-1} $Å^{-1}$ reached for all of the atoms. The molecular mechanics (MM) method-based interaction energy for each of these energy-minimized 20 candidates was calculated according to the following equations,

$$\Delta E_{MM} = E_{complex} - E_{DAT} - E_{DA}, \quad (1)$$

$$\Delta E_{MM} = \Delta E_{ele} + \Delta E_{vdw}, \quad (2)$$

where ΔE_{MM} is the binding energy contributed from electrostatic and van der Waals interactions; $E_{complex}$, E_{DAT}, and E_{DA} were the energies of the complex, free DAT, and free dopamine, respectively. All these terms were calculated with the Sander module of the AMBER8 program (46). By this way of ranking and checking of geometric match quality, two complex structures were selected as the final candidates, and then subjected to more accurate binding free energy calculations by using the molecular mechanics-Poisson-Boltzmann surface area (MM-PBSA) method (51).

In the MM-PBSA calculations, the free energy of dopamine binding, ΔG_{bind}, is calculated from the difference between the free energies of the complex ($G_{complex}$), the free DAT (G_{DAT}), and free dopamine (G_{DA}) as Eq. 3:

$$\Delta G_{\text{bind}} = G_{\text{complex}} - (G_{\text{DAT}} + G_{\text{DA}}). \quad (3)$$

The ΔG_{bind} was evaluated as a sum of the changes in the MM gas-phase binding energy (ΔE_{bind}), solvation free energy (ΔG_{solv}), and entropy contribution ($-T\Delta S$),

$$\Delta G_{\text{bind}} = \Delta E_{\text{bind}} - T\Delta S, \quad (4)$$

$$\Delta E_{\text{bind}} = \Delta E_{\text{MM}} + \Delta G_{\text{solv}}, \quad (5)$$

$$\Delta G_{\text{solv}} = \Delta G_{\text{PB}} + \Delta G_{\text{np}}, \quad (6)$$

$$\Delta G_{\text{np}} = \gamma SASA. \quad (7)$$

Electrostatic solvation free energy was calculated by the finite-difference solution to the Poisson-Boltzmann (PB) equation (ΔG_{PB}) as implemented in the Delphi program (52,53). The dielectric constants used were 1 for the solute and 78.5 for the solvent. The SASA was calculated by the default surface area calculation program in the MM-PBSA module of AMBER8 program (46) with the default $\gamma = 0.0072$ kcal Å^{-2}. In the MM-PBSA calculations, the lipid molecules were treated as part of the solute because DAT is a membrane protein. Keeping lipid molecules as part of the ''solute'' are helpful to reduce some possible systematic errors, especially for the calculation of ΔG_{PB}. To avoid the insufficient accuracy of solvation energy calculation for metal ions by Delphi program, the two bound Na^+ ions were removed only when calculating ΔG_{PB}. The entropy contribution, $-T\Delta S$, to the binding free energy was calculated at $T = 300$ K by using the Nmode module of the AMBER8 program (46), which is based on a combination of the standard classical statistical formulas and normal mode analysis (54,55).

After the calculation of binding free energy, one of the two candidate structures was selected as the final DAT-dopamine complex based on its much lower binding free energy and higher quality of structural matching.

Molecular dynamics simulations

To explore the possible substrate-entry pathway, MD simulations were performed on the aforementioned DAT system by using the Sander module of AMBER8 (46). MD simulations were performed also for the purpose of making the extracellular loop 2 more reasonably folded after a sequence of 25 residues was inserted during the modeling of DAT structure. The whole system was gradually heated to 300 K by weak-coupling method (56,57) and equilibrated for ~49 ps. Throughout the MD simulations, a 12 Å nonbonded interaction cutoff was used and the nonbonded list was updated every 1000 steps. The particle-mesh Ewald method (58,59) was applied to treat long-range electrostatic interactions. The lengths of bonds involving hydrogen atoms were fixed with the SHAKE algorithm (60), enabling the use of a 2-fs time step to numerically integrate the equations of motion. Finally, the production MD was kept running ~2.167 ns with a periodic boundary condition in the NTP ensemble at $T = 300$ K with Berendsen temperature coupling and at $P = 1$ atm with anisotropic molecule-based scaling (56,57).

Similar MD simulations were also performed for 2.476 ns on the constructed DAT-dopamine complex for the purpose of further relaxation of the structure.

Most of the MD simulations were performed on the HP supercomputers (Superdome SDX and Linux cluster XC) at University of Kentucky Center for Computational Sciences. The other computations were carried out on SGI Fuel workstations and a 34-processor IBM x335 Linux cluster in our own lab.

RESULTS AND DISCUSSION

Structural model of DAT

The amino-acid sequence alignment between human DAT and $LeuT_{Aa}$ (Fig. 1) shows that 12 regions with high homology can be assigned to 12 α-helices. The assembly of these helices in a biological environment (Fig. 2 *A*) is structurally organized similar to the template $LeuT_{Aa}$ (34). The whole model appeared to be a shallow glasslike shape opening toward the extracellular side and a pseudo-twofold axis between helices 1–5 and helices 6–10. The energy-minimized DAT structure (Fig. 2) has a root-mean-square deviation (RMSD) of 0.13 Å for Cα atoms and 0.69 Å for all heavy atoms from the initial structural model. Compared with the template $LeuT_{Aa}$ structure (34), the RMSD for Cα atoms of 12 transmembrane helices was only 0.52 Å. These small structural deviations suggest a high fidelity for the structure prediction of DAT. Like other bacterial homologs in the same family (61), the first 10 helices of DAT should act as the essential core structure for Na^+/Cl^--dependent transporting. With

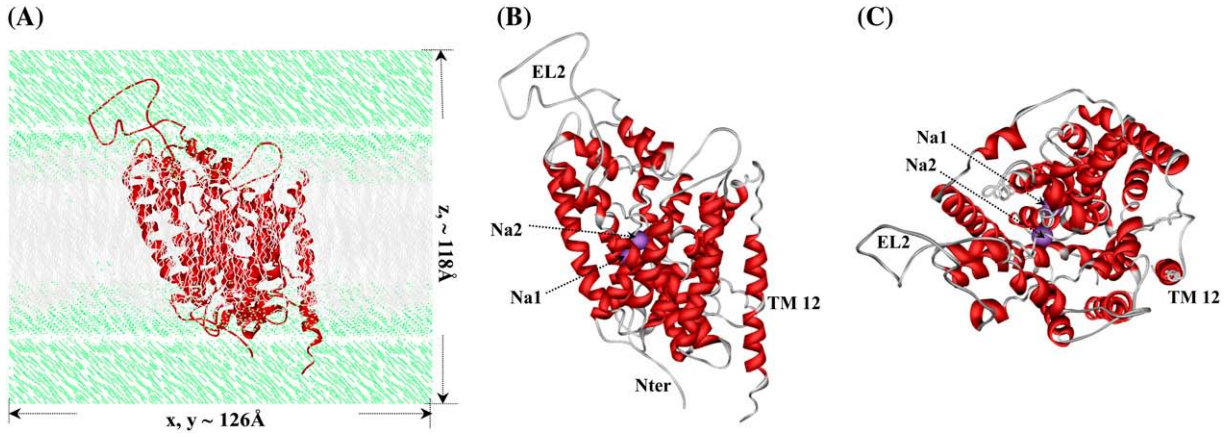

FIGURE 2 Initial structural model of human DAT in the physiological environment used for MD simulations. (*A*) DAT protein is represented as ribbon in red, lipid molecules in gray, and water molecules in green. Labeled also are the system sizes along *x*, *y*, and *z* axes. (*B*) Top view of DAT protein itself shown as ribbon in red, and Na^+ ions as CPK in magenta. The Na^+ ions, extracellular loop 2 (*EL2*), transmembrane helix 12 (*TM12*), and Nter are labeled. (*C*) Side view of DAT protein.

inverted V-shape, helices 9 and 10 hold helices 3 and 8 like a pincer. By flanking the outer surfaces of helices 9 and 10, helix 12 protrudes the deepest into the intracellular side. Together with helix 9, helix 12 is situated probably at the interface of DAT dimer or other possible oligomers such as the tetramer (62,63).

Our MD-simulated DAT model is considerably different from the previously reported DAT models (35,36). The major difference exists not only in the starting position and the length of each helix, but also in the assembly of 12 transmembrane helices. Furthermore, the second substrate (i.e., the two Na^+ ions) (31) was not considered in the previous DAT models. These differences between the previous models and our current model are mainly due to the fact that the more reasonable template (34) was used in our DAT structure prediction. As noted above, the template (i.e., the structure of $LeuT_{Aa}$) used to build our model is in the same NSS family to which DAT belongs, whereas the previous models (35,36) were constructed from different templates, one from the Na^+/H^+ antiporter, and another from Lactose permease (31). The Na^+/H^+ antiporter and Lactose permease belong to different families of the ion-coupled secondary transporters superfamily; neither of these two templates shares the same family with DAT. In addition, the effects of the lipid bilayer and solvent molecules on the DAT structure were also accounted for in the structural optimization process (Fig. 2 *A*). The energy minimization on the system including the lipid bilayer and solvent molecules helped to improve the quality of interhelical packing and the helix-bilayer packing. The obtained model structure (Fig. 2) should be more reasonable than the previous models obtained from the in-vacuum modeling (35,36) In general, the existence of the membrane bilayer and solvent molecules is crucial for maintaining the proper folding of membrane proteins and their reasonable conformational changes necessary for the normal protein functions (64).

Based on the Cα RMSD changes during the MD simulation (*black curve* in Fig. 3 *A*), one can see that the optimized DAT structure became further relaxed after ~0.4 ns of the significant structural perturbation. Such structural change during 0~0.4 ns may be attributed to the dynamic packing effect by lipid molecules on the relative assembly of DAT helices. After ~0.4 ns, the helix assembly of DAT became relatively stable as the Cα RMSD curve became quite flat.

It is interesting to track the distance change between the positively charged side-chain atoms of Arg^{85} from helix 1 and the negatively charged side-chain atoms of Asp^{476} from helix 8 during the MD simulation (*black curve* in Fig. 3 *B*). As noted in the x-ray structure of $LeuT_{Aa}$ (34), these two residues may also form an ion-pair in DAT without a substrate, and this ion-pair was supposed to be the major obstacle when the substrate is on the way to enter the binding pocket. There were hydrogen-bonding and strong electrostatic interactions between Arg^{85} and Asp^{476} in the starting DAT structure used for the MD simulation. During the MD simulation, the minimum distance between the side chains of these two residues became much larger and there was a very large fluctuation of the distance, indicating that the Arg^{85}-Asp^{476} pair (salt bridge) was seldomly formed during the MD simulation and easy to be separated (Fig. 3 *B*).

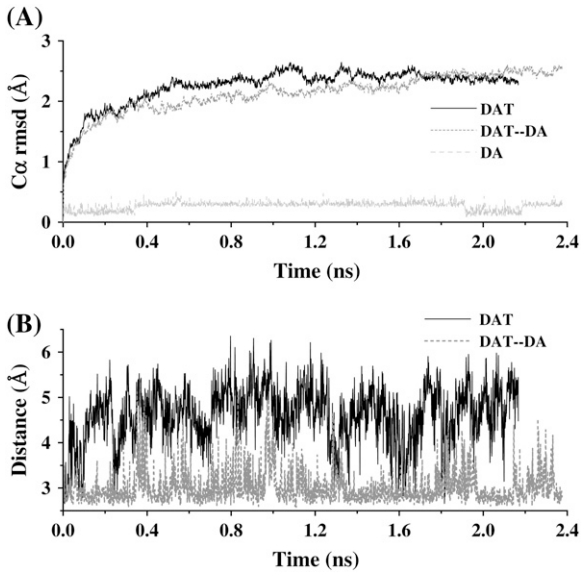

FIGURE 3 Plots of the Cα RMSD and key distances in the simulated DAT and DAT-dopamine structures versus the simulation time (nanoseconds) during the MD simulations. (*A*) The DAT Cα RMSD, the Cα RMSD of the DAT-dopamine complex, and the RMSD of dopamine (DA) in the complex. (*B*) The minimum-distance changes between the positively charged side-chain atoms (NE, NH1, and NH2) of Arg^{85} and the negatively charged side-chain atoms (OD1 and OD2) of Asp^{476} in both the DAT and DAT-dopamine complex.

The Na^+ ions were bound on the midpoint of the membrane, roughly around the unwound regions of helices 1 and 6 (Fig. 2, *B* and *C*). The major role of these two Na^+ ions may be considered to stabilize the DAT core structure and the unwound helices 1 and 6. The two Na^+ ions may also help to turn the DAT to externally facing form, thus allowing the access of the substrate to its binding site (16,17,20). In our starting structure of DAT used in the MD simulation, the first Na^+ (denoted by Na1 in Fig. 2, *B* and *C*) was coordinated with the carbonyl oxygen of Ala^{77} (helix 1), side-chain carbonyl oxygen of Asn^{82} (helix 1), backbone carbonyl oxygen and side-chain hydroxyl oxygen of Ser^{321} (helix 6), and carbonyl oxygen of Asn^{353} (helix 7). In $LeuT_{Aa}$ (34), the sixth coordination of the corresponding Na^+ was from the carboxyl oxygen of the substrate. Correspondingly, the space around the sixth coordination of Na1 in DAT was squeezed by the surrounding backbone atoms. Tracking the coordination information in the MD trajectory, we found that the most conserved residues Ala^{77}, Asn^{82}, and Asn^{353} (Figs. 1 and 4 *A*) were always the ligands of Na1 (Table 1). Ser^{321} coordinated Na1 through its backbone carbonyl oxygen, but the coordination of its side-chain hydroxyl oxygen was replaced by the

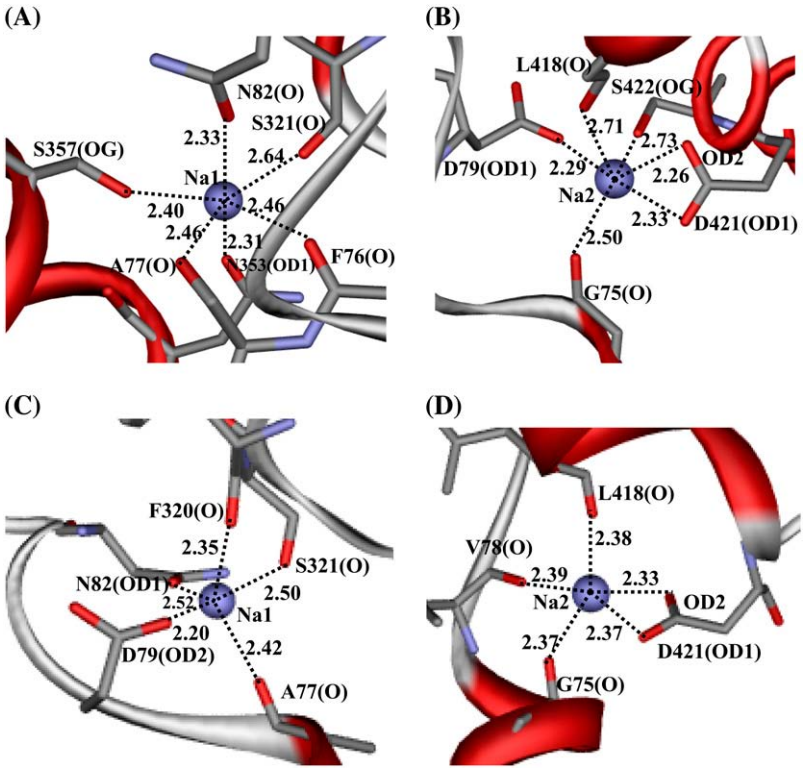

FIGURE 4 Representative local structures of DAT surrounding the Na^+ ions (i.e., Na1 and Na2) captured at 1.50 ns snapshot of the MD simulations on DAT (*A* for Na1 and *B* for Na2) and DAT-dopamine complex (*C* for Na1 and *D* for Na2). In all cases, Na^+ ions are shown in CPK style. The coordinating residues are shown in stick, and the protein in ribbon, representation. The coordinating distances are labeled.

side-chain hydroxyl oxygen of Ser^{357}. Further coordination by the backbone carboxyl oxygen of Phe^{76} made Na1 saturated to the typical hexacoordination and thus Na1 was stabilized in its binding site. During the MD simulation, Na1 had a fraction of 0.580 for hexacoordination and a fraction of 0.397 for pentacoordination. As shown in Fig. 4 *A*, for a typical DAT structure at 1.50-ns snapshot of the MD trajectory, most of the coordinating atoms interact with Na1

TABLE 1 Coordination details for the Na^+ ions during the MD simulations for both the DAT model and its complex structure with dopamine

	DAT			DAT-dopamine complex		
Ions	Residue	Atom	Fraction	Residue	Atom	Fraction
Na1	Phe^{76}	O=C	0.735	Ala^{77}	O=C	1.000
	Ala^{77}	O=C	0.988	Asp^{79}	OD2	1.000
	Asn^{82}	OD1	0.998	Asn^{82}	OD1	1.000
	Ser^{321}	O=C	0.991	Phe^{320}	O=C	0.995
	Asn^{353}	O=C	1.000	Ser^{321}	O=C	0.944
	Ser^{357}	OG	0.965			
	Ser^{321}	OG	0.091			
	Coordination No. and its fraction		5: 0.397 6: 0.580	Coordination No. and its fraction		4: 0.006 5: 0.963 6: 0.030
Na2	Gly^{75}	O=C	0.965	Gly^{75}	O=C	1.000
	Asp^{79}	OD1	0.948	Val^{78}	O=C	1.000
	Leu^{418}	O=C	0.911	Leu^{418}	O=C	0.994
	Asp^{421}	OD1	1.000	Asp^{421}	OD1	1.000
	Asp^{421}	OD2	0.963	Asp^{421}	OD2	1.000
	Ser^{422}	OG	0.741			
	Val^{78}	O=C	0.032			
	Coordination No. and its fraction		5: 0.200 6: 0.780	Coordination No. and its fraction		4: 0.045 5: 0.949

A distance cutoff of 3 Å was used for the coordination criterion, and the fraction was calculated as the ratio of the number of snapshots with the coordination to the total number of snapshots taken from the stable MD trajectory. The fraction of each coordination number (4, 5, or 6) was calculated similarly.

within an internuclear distance of 2.5 Å, except the backbone carbonyl oxygen of Ser^{321} with a distance of 2.64 Å. The details of the coordination for Na1 revealed in this MD simulation on DAT structure are all consistent with the observations from experimental studies for the existence of Na1 and its coupling with the substrate binding in DAT and SERT, suggesting a general structural feature around Na1 for NSS transporters (16,17,34).

The ligands of the second Na^+ (denoted by Na2 in Fig. 2, *B* and *C*, and Fig. 4 *B*) in the starting DAT structure used in the MD simulation were mostly the backbone carbonyl oxygen atoms. These ligands were the carbonyl oxygen atoms of Gly^{75} (helix 1), Val^{78} (helix 1), and Leu^{418} (helix 8), the side chain OD1 of Asp^{79} (helix 1), and the side-chain atoms OD1 and OD2 of Asp^{421} (helix 8). As shown in Table 1 and Fig. 4 *B*, the most conserved residues Gly^{75} and Asp^{79} and the conservatively substituted Leu^{418} had very high fractions of the coordination to Na2 with short coordinating distances. Asp^{421} always coordinated to Na2 through the negatively charged side-chain atoms OD1 and OD2, which was the main source of electrostatic interactions. The coordination to Na2 by the side-chain hydroxyl oxygen of Ser^{422} was sometimes replaced by the backbone carbonyl oxygen of Val^{78}, which only had a very small fraction of the coordination. The fraction of hexacoordination for Na2 was larger than that for Na1 by ~0.200, as seen in Table 1.

Complex model of DAT binding with dopamine

The dopamine-binding site in DAT was made by unwound regions of helices 1 and 6 and helices 3 and 8, which was close to the sites of Na^+-binding, as seen in Fig. 5 *A*. In a typical structure of the MD-simulated DAT-dopamine complex at the 1.50-ns snapshot of the MD trajectory, dopamine was located in a totally dehydrated pocket (Fig. 5 *B*). The cationic head of dopamine was partially neutralized by the helix dipoles at the unwound regions of helices 1 and 6, and the negatively charged side chain of Asp^{79} from helix 1.

The dynamic behavior of the DAT-dopamine complex has been monitored by the Cα RMSD changes (Fig. 3 *A*), the Arg^{85}-Asp^{476} paring (Fig. 3 *B*), the coordination information of Na^+ ions (Fig. 4, *C* and *D* and Table 1), and the key distances from dopamine to several closely contacted residues and Na^+ ions (Fig. 6). As shown in Fig. 3 *A*, during the first 2 ns of the MD simulation, the Cα RMSD change of DAT-dopamine complex was much smaller than that of the corresponding DAT structure without dopamine. More interestingly, Arg^{85} and Asp^{476} became a stable ion pair, as tracked by the minimum distance between the charged side chains of this pair of residues (Fig. 3 *B*), as the distance was <3 Å, at most, of the snapshots. These dynamic changes reveal that the Na^+-bound DAT was stabilized by the binding of dopamine. In other words, the Na^+-bound DAT can easily accept dopamine as a substrate. After binding with dopamine, the local intermolecular contacts became quite stable during the MD simulation (Fig. 6 *A*), although the Cα RMSD changes depicted in Fig. 3 *A* suggested a certain extent of backbone motion for the complex structure.

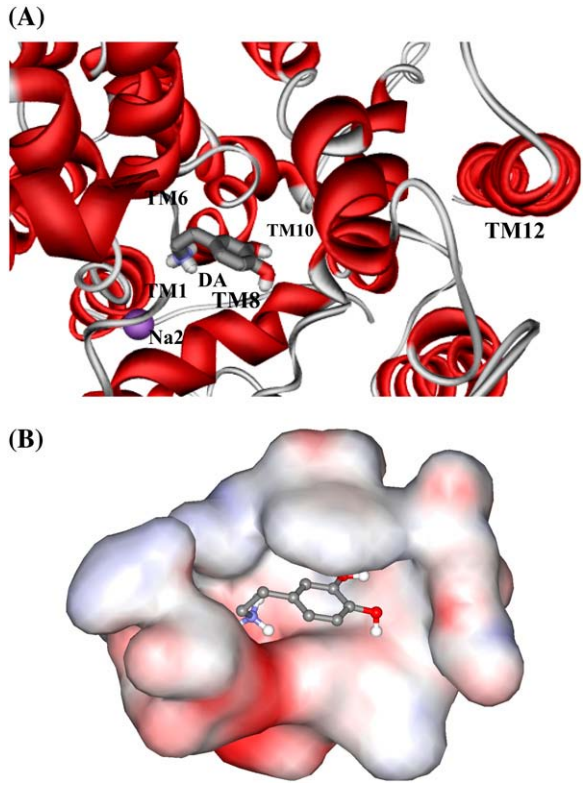

FIGURE 5 Typical structure of the DAT-dopamine binding complex, which was the 1.50 ns snapshot of the MD trajectory. (*A*) Viewing the dopamine molecule (shown as ball-and-stick) in the complex model from the extracellular side. Only part of the DAT is shown as ribbon in red, and Na2 as CPK in magenta. Helices 1, 6, 8, 10, and 12 are labeled to indicate the relative position of dopamine in DAT. (*B*) Viewing the DAT in the binding pocket in the same orientation as panel *A*. The binding pocket is represented in molecular surface format, colored with electrostatic potentials in which blue is for positive and red is for negative potentials.

The coordination of Na1 was perturbed by the binding of dopamine. As listed in Table 1, Na1 kept Ala^{77} and Asn^{82} as its ligands, and it lost the coordination from Phe^{76}, Asn^{353}, and Ser^{357}, while Asp^{79} and Phe^{320} became the new ligands of Na1. Meanwhile, Ser^{321} also restored its role as a ligand of Na1 (Fig. 4 *C*). It is worth noting that Asp^{79} switched its role from coordinating Na2 through its side chain OD1 in the DAT structure without dopamine to coordinating Na1 through its side chain OD2 in the DAT-dopamine complex. This was the most remarkable change in the local binding environment after the binding with dopamine, suggesting an indispensable role of this charged residue in the process of substrate-binding to DAT. Concerning the coordination of Na2, after the dopamine binding to DAT, the OD1 atom of Asp^{79} no longer coordinated to Na2 while its OD2 atom coordinated the Na1. The coordination of Na2 from the OD1 of Asp^{79} in the DAT structure without dopamine was

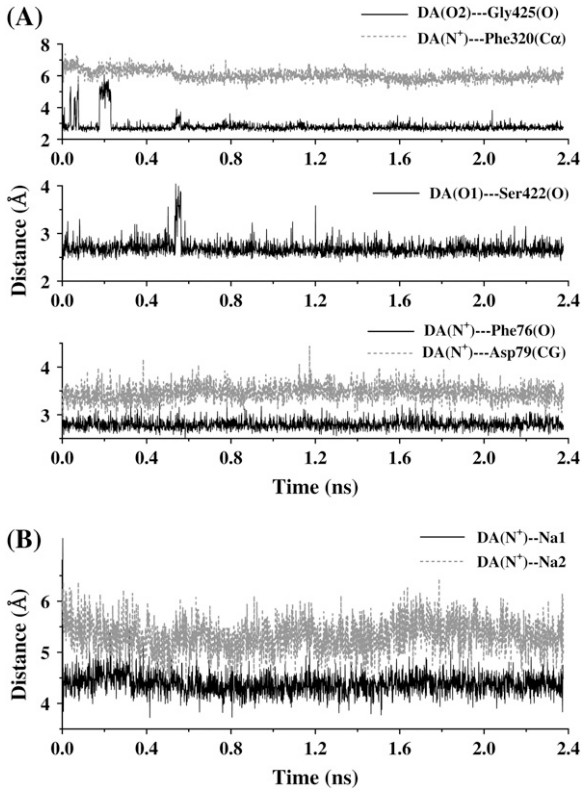

FIGURE 6 (*A*) Distances from the atoms (the nitrogen and hydroxyl oxygen atoms) of dopamine to the carbonyl oxygen of Phe^{76}, side chain CG of Asp^{79}, Cα of Phe^{320}, carbonyl oxygen of Ser^{422}, and carbonyl oxygen of Gly^{425}. (*B*) Distances from the cationic head of dopamine to the bound Na^+ ions as observed during the MD simulation of the DAT-dopamine complex.

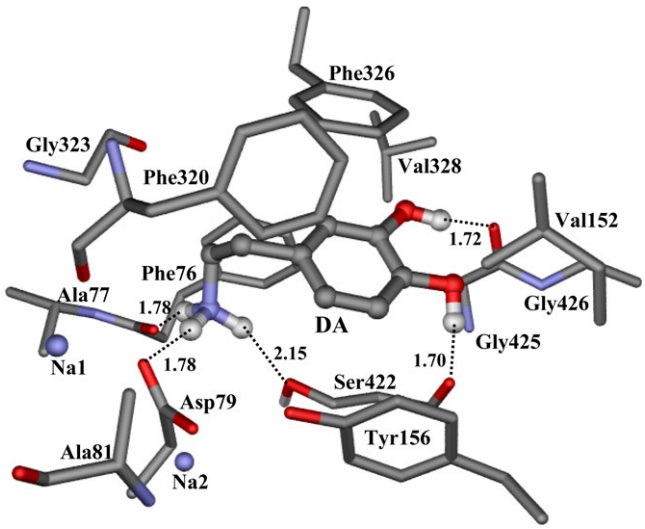

FIGURE 7 Representative molecular interactions between dopamine and DAT, taken at the 1.50-ns snapshot of the MD-simulated DAT-dopamine complex. Residues from DAT within 5 Å of dopamine are labeled and shown in stick style, while dopamine is shown in ball-and-stick. Critical hydrogen-bonding interactions between dopamine and DAT are represented as dash lines with labeled distances, also labeled the bound Na^+ ions (Na1 and Na2).

replaced by the backbone carbonyl oxygen of Val^{78} (Fig. 4 *D*) in the simulated DAT-dopamine complex. Na2 kept its coordination from Gly^{75}, Leu^{418}, and Asp^{421}, but its coordination from Ser^{422} was lost. Another significant change was the coordination numbers of both Na^+ ions after the dopamine binding, i.e., from 6 in the DAT structure without dopamine to 5 in the DAT-dopamine complex (Table 1). The decreased coordination numbers of both Na^+ ions can be attributed to both the steric and electrostatic effects of the positively charged dopamine. The MD-simulated average distances from the cationic head of dopamine to Na1 and Na2 (Fig. 6 *B*) were ~4.5 Å and ~5.5 Å, respectively. On the other hand, the repulsion between the positive charges was neutralized by the negatively charged Asp^{79} and partially by the surrounding helix dipoles.

The detailed atomic interactions between dopamine and DAT are featured as electrostatic, hydrogen bonding, and hydrophobic contacts, as shown in Fig. 7 for a typical structure of the MD-simulated complex at the 1.50 ns snapshot. The hydrogen atoms on the positively charged head of dopamine formed three hydrogen bonds with DAT. One hydrogen bond was formed with the backbone carbonyl oxygen of Phe^{76} from helix 1, the second was formed with the side chain OD2 of Asp^{79} from helix 1, and the third with the side-chain hydroxyl oxygen of Ser^{422} from helix 8. Meanwhile, the side-chain hydroxyl group of Ser^{422} had a hydrogen bond with the side chain OD2 of Asp^{421}. The distance from the positively charged head of dopamine to the center of the aromatic side chain of Phe^{76} was as short as 4.18 Å. The nearest hydrogen atom on the cationic head of dopamine had a distance of 3.83 Å with the aromatic side chain of Phe^{76}, indicating a cation-π interaction. The role of Asp^{79} from helix 1 was twofold. The side chain OD2 of Asp^{79} coordinated to Na1 and hydrogen-bonded to the cationic head of dopamine, while its side chain OD1 hydrogen-bonded to the side-chain hydroxyl group of Tyr^{156} from helix 3. The average distances from the nitrogen atom of the positively charged head of dopamine to the OD1 and OD2 atoms of Asp^{79} are within the range of effective electrostatic interactions (2.79 Å and 4.16 Å, respectively). The aromatic side chain of Tyr^{156} was in close side packing with the aromatic ring of dopamine (Fig. 7). Such strong interactions between dopamine and the side chains of Asp^{79}, Tyr^{156,} and Ser^{422} should be the major binding forces anchoring dopamine to its binding site. Tyr^{156} is a strictly conserved residue between all members in the NSS family (Fig. 1), and Ser^{422} is also conservative. Therefore, the mutual interactions between the side chains of Tyr^{156} and Asp^{79} may act as a latch to stabilize the irregular structure around the unwound region of helix 1. The involvement of Asp^{79} in the vital local interactions with both dopamine and Na^+ can explain why mutations Asp^{79}Ala, Asp^{79}Gly, and Asp^{79}Glu dramatically reduced dopamine reuptake as demonstrated in previously reported experimental studies on DAT

(18,19). The mode of electrostatic attraction plus hydrogen bonding between Asp^{79} and the positively charged head of dopamine is also supported by a recent mutational study on the Asp^{79}Glu mutant of DAT (24). The corresponding position of Tyr^{156} in other members of the NSS family has also been indicated in the substrate binding and translocation, such as in serotonin transporter and γ-aminobutyric acid transporter (65–67). The substrate binding was not investigated in the previous modeling studies on DAT (35,36).

In addition, the hydroxyl groups of dopamine formed two hydrogen bonds with DAT, one with the backbone carbonyl oxygen of Ser^{422} and the other with the backbone carbonyl oxygen of Gly^{425} from helix 8. These two hydrogen bonds helped to orient the aromatic ring of dopamine in better parallel packing with the aromatic side chain of Phe^{326} from helix 6. Additional hydrophobic contacts between dopamine and DAT came from the hydrophobic side chains of several other residues. Side chains of Ala^{77}, Ala^{81}, and Phe^{320} interact with the alkyl chain of dopamine between its cationic head and aromatic ring. Gly^{426} and side chains of Val^{152} and Val^{328} added more contacts with the aromatic ring of dopamine.

As observed from the MD simulation, Phe^{76}, Asp^{79}, Ser^{422}, and Gly^{425} had strong hydrogen-bonding interactions with the cationic head and hydroxyl groups of dopamine (Table 2). The total fraction of hydrogen bonding for each of these residues is always over 0.95 during the 2.476 ns MD simulation.

Comparison with available site-directed mutagenesis studies

Our modeled structures of DAT and its binding with dopamine can be used to understand the experimental results obtained from previously reported site-directed mutagenesis studies (18,19,22,28). As discussed above, according to our DAT model, the negatively charged atoms at the side chain of Asp^{79} interact with the cationic head of dopamine through the direct hydrogen-bonding and electrostatic interactions. Mutations on this residues, such as Asp^{79}Ala and Asp^{79}Gly, are expected to abolish these crucial interactions, and thus these mutations lead to the loss of the dopamine-reuptake function as reported by Uhl et al. (18). Asp^{79}Glu mutation is also expected to significantly weaken its interactions with the cationic head of dopamine and the two Na^+ ions, which explains why this mutation also dramatically reduced the dopamine reuptake (18). As reported also by Uhl et al. (19), Phe^{155}Ala mutation caused only 3% decrease in the binding affinity of dopamine. According to our model of DAT in complex with dopamine, Phe^{155} is located just above the dopamine binding pocket, and the shortest internuclear distance between Phe^{155} and dopamine is >5 Å. The possible hydrophobic interaction between Phe^{155} with dopamine should be very weak, making this residue much less important than other residues inside the dopamine-binding pocket.

It has been known that Asp^{313}Asn mutation decreased the K_m for dopamine binding with DAT by sixfold (22), whereas Lys^{257}A and Arg^{283}Ala mutations increased the K_m for dopamine binding with DAT by sixfold and threefold, respectively (28). Based on our modeled structures, the distance between the negatively charged atoms of Asp^{313} side chain and the cationic head of dopamine is ~8 Å, whereas the distances from the cationic head of dopamine to the positively charged atoms of Lys^{257} and Arg^{283} side chains are ~10 Å and ~11 Å, respectively. In consideration of the long-range electrostatic interactions between the charged dopamine and these charged residues, with the Asp^{313}Asn mutation, the net

TABLE 2 The hydrogen-bonding (HB) interactions between DAT and dopamine in the MD-simulated DAT-dopamine complex

Residue	Donor	Acceptor	Residue	HB_{dist} (Å) (SD)	Fraction
DA	N1-H3	O=C	Phe^{76}	2.796 (0.11)	0.731
DA	N1-H5	O=C	Phe^{76}	2.794 (0.10)	0.258
DA	N1-H5	OD2	Asp^{79}	2.839 (0.12)	0.732
DA	N1-H4	OD2	Asp^{79}	2.850 (0.13))	0.253
DA	N1-H4	OG	Ser^{422}	2.987 (0.15)	0.618
DA	N1-H3	OG	Ser^{422}	2.976 (0.17)	0.211
DA	O1-H10	O=C	Ser^{422}	2.672 (0.11)	0.979
DA	O1-H10	O=C	Gly^{425}	2.360 (0.15))	0.024
DA	O2-H11	O=C	Gly^{425}	2.745 (0.14)	0.953

The criteria/cutoffs used for the HB counting was 3.5 Å for the distance (HB_{dist}) between the donor and acceptor atoms and 110° for the HB angle along the donor, hydrogen, and the acceptor. The HB fraction was calculated as the ratio of the number of snapshots with the HB to the number of total snapshots collected. All HB pairs with fractions over 1% and their average HB_{dist} values are listed with the standard deviations (SD) in parentheses. See scheme below.

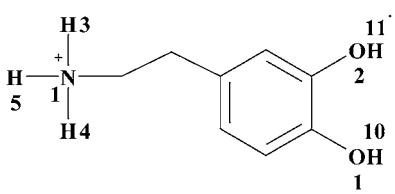

charge of the residue changes from −1 to 0 and, therefore, the favorable electrostatic attraction between Asp^{313} and dopamine is expected to vanish. With the Lys^{257} or Arg^{283} mutation, the net charge of the residue changes from +1 to 0 and, therefore, the unfavorable electrostatic repulsion between the residues and dopamine is expected to disappear. These results qualitatively explain why the Asp^{313}Asn mutation decreased the K_m for dopamine binding with DAT (22), whereas Lys^{257}A and Arg^{283}Ala mutations increased the K_m for dopamine binding with DAT (28).

As observed in previously reported experimental studies, the Trp^{84}Leu mutation on helix 1 and the Leu^{104}Val, Phe^{105}Cys, and Ala^{109}Val mutations on helix 2 had no obvious effects on the K_m value for dopamine binding with DAT (22,25,26). This is because these residues are far away from the dopamine-binding site according to our modeled structures. In addition, based on our modeled structures and the MD simulations trajectory, amino-acid residues His^{375} to Ile^{379} at the extracellular end of helix 7 belong to a loop and residue Glu^{396} is at the beginning of helix 8. Such a structural feature is also consistent with the key distances determined in a study of the structure-function relationship by performing the Zn^{2+}-site engineering (20).

Binding free energy

In the MM-PBSA calculation of the binding free energy for the DAT-dopamine binding using the modeled structure before the MD simulation, we obtained $\Delta E_{bind} = -21.6$ kcal/mol and $-T\Delta S = 16.0$ kcal/mol at $T = 298.15$ K. Thus, the binding free energy (ΔG_{bind}) between dopamine and DAT was calculated to be –5.6 kcal/mol by using the DAT structure before the MD simulation. Based on the calculated ΔG_{bind} value, the dissociation constant (K_d) for the DAT-dopamine complex is estimated to be 7.8×10^{-5} M (or 78 μM). We also calculated the binding free energy by using the MD-simulated DAT-dopamine structure. The MM-PBSA calculations were performed on 120 snapshots (i.e., one snapshot per 10 ps) taken from the last 1.2 ns of the MD trajectory (see Fig. 3 *A*). For each of these 120 snapshot structures, we carried out the calculations on both the gas-phase binding energy and the solvent shift. The final results were taken as the averages of the corresponding energetic values calculated with the 120 snapshots. Based on the calculated results, the binding energy shift due to the MD simulation was determined to be –0.8 kcal/mol, i.e., ΔG_{bind} (after MD) = –5.6 − 0.8 = −6.4 kcal/mol. Based on the ΔG_{bind} value of –6.4 kcal/mol, the dissociation constant (K_d) is evaluated to be 20 μM, which is closer to the experimental ΔG_{bind} value of –7.4 kcal/mol derived from the experimental K_M value of 3.466 ± 0.200 μM (28). The deviation (~1.0 kcal/mol) of the calculated binding affinity from the experimental value may be attributed to the approximations inherent in MM-PBSA method (51). For example, explicit solvent molecules were employed in the optimization and MD simulations of the DAT-dopamine complex model, but were subsequently replaced with a continuum solvent model in the calculation of the solvation free energy contribution (ΔG_{solv}) through solving the PB equation (52,53). A recently reported computational study (68) also demonstrated that the MM-PBSA method could significantly underestimate the binding free energy.

Substrate-entry pathway

Based on the MD-simulated DAT-dopamine complex structure, a top view on the dopamine binding site from the extracellular side shows that dopamine was positioned inside a hydrophobic pocket (Fig. 5). The cradlelike pocket was covered by the aromatic side chains of Phe^{320} and Phe^{326} and the hydrophobic side chain of Val^{152} (Figs. 7 and 8). This top cover of the binding pocket was further stacked by the side chains of Phe^{155} from helix 3, Arg^{85} from helix 1, and Asp^{476} from helix 10. Although the charged side-chain atoms of residues Arg^{85} and Asp^{476} were seldomly in direct charge-charge interactions, as indicated in the MD simulation on

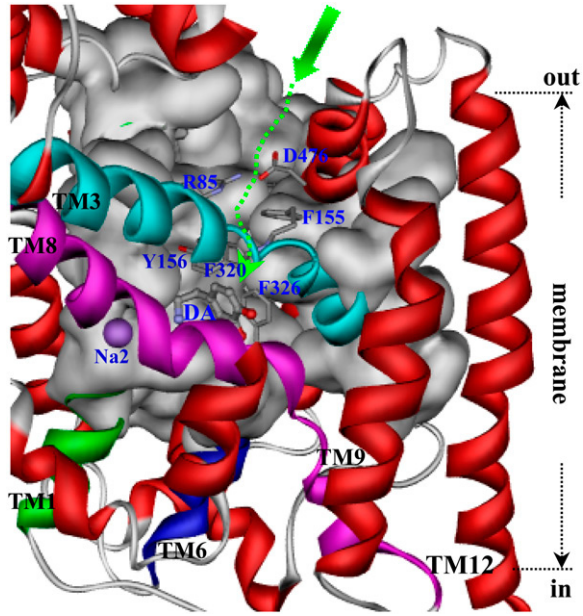

FIGURE 8 Side view of the proposed dopamine-entry pathway in DAT with TM12 parallel to the normal of the membrane. The protein is shown as ribbon with helix 1 in green, helix 3 in cyan, helix 6 in blue, helix 8 in magenta, and other helices in red. With helices 3 and 8 in front, the back wall of the pathway is represented by molecular surface in gray, and residues 220–241 are not shown for clear view of the pathway back wall. The relative position of the membrane bilayer is indicated. The proposed substrate-entry pathway starts from the extracellular side as indicated by the large green arrow, going down inside the tunnel along the dashed green arrow to the binding pocket. The side chains of residues on the way of the tunnel to the binding pocket are shown in stick representation and labeled in blue. These are the salt-bridge pair of Arg^{85} and Asp^{476}, aromatic residues as Phe^{155}, Ty^{156}, Phe^{320}, and Phe^{326}. Dopamine is labeled as DA and the second Na^+ as Na2 in blue.

DAT (*black curve* in Fig. 3 *B*), the mutual interactions between these two residues were probably mediated by the surrounding solvent water molecules. These two charged residues were just over the top of Phe^{326} from helix 6. The NH groups of Arg^{85} side chain also formed a hydrogen bond with the carbonyl oxygen on the side chain of Gln^{317} from helix 6. Except these intramolecular interactions, the funnel-like tunnel formed by the helices 1, 3, 6, 8, and 10 was quite opening toward the extracellular side of the membrane bilayer (Fig. 7).

Considering the unwinding features of helices 1 and 6 around the midpoint of the membrane, it is not difficult for the up-half of helices 1 and 6 to move apart or toward each other by using the unwound regions of these two helices as the joint points. Such unique flexibility of the substrate-binding domain of DAT affords a possible, reasonable pathway for the entry of Na^+ ions and substrate dopamine toward their binding sites. That is, once captured near the mouth in the extracellular side of DAT, dopamine molecule can slide down to the door of binding pocket (*dashed green arrow* in Fig. 8). By the help of electrostatic attraction from Asp^{476}, the entering of dopamine probably brings about local motion of the up-half of helices 1 and 6. After further sliding of dopamine molecule toward the binding pocket, the charged atoms of Arg^{85} and Asp^{476} come closer to each other. In coupling with the dopamine molecule orientating in the binding pocket, the coordinations of both Na^+ ions are adjusted. As a balance, the Arg^{85}-Asp^{476} salt bridge is formed (Fig. 3 *B*), thus stabilizing the whole complex structure (Figs. 6 and 7).

CONCLUSION

This computational modeling, molecular docking, and molecular dynamics simulations have led us to develop a reasonable three-dimensional (3D) structural model of dopamine transporter (DAT) and its binding dopamine. Our modeled 3D structures of DAT and its complex with dopamine have provided some detailed structural and mechanistic insights concerning how DAT interacts with its substrates at atomic level, extending our mechanistic understanding of DAT modulating the dopamine reuptake with the help of Na^+ ions. The general features of our modeled 3D structures are consistent with all of the available experimental data. Based on the modeled 3D structures, our calculated binding free energy for dopamine binding with DAT is also reasonably close to the experimentally measured binding affinity. Finally, a possible substrate-entry pathway, which involves the formation and breaking of the Arg^{85}-Asp^{476} salt bridge, is proposed according to the results obtained from the modeling and MD simulation. The new structural and mechanistic insights obtained from this computational study should be valuable for design of future, further biochemical and pharmacological studies on the detailed structures and mechanisms of DAT and other homologous members of the neurotransmitter sodium symporters (NSS) family.

The authors acknowledge the Center for Computational Sciences at the University of Kentucky for supercomputing time on Superdome (a shared-memory supercomputer, with four nodes for 256 processors).

The research was supported by the National Institutes of Health/National Institute on Drug Abuse (grant No. R01 DA013930 to C.-G. Z.).

REFERENCES

1. Uhl, R. G. 2003. Dopamine transporters: basic science and human variation of a key molecule for dopaminergic function, locomotion, and Parkinsonism. *Mov. Disord.* 18:S71–S80.
2. Mendelson, J. H., and N. K. Mello. 1996. Management of cocaine abuse and dependence. *N. Engl. J. Med.* 334:965–972.
3. Singh, S. 2000. Chemistry, design, and structure-activity relationship of cocaine antagonists. *Chem. Rev.* 100:925–1024.
4. Paula, S., M. R. Tabet, C. D. Farr, A. B. Norman, and W. J. Jr. Ball. 2004. Three-dimensional quantitative structure-activity relationship modeling of cocaine binding by a novel human monoclonal antibody. *J. Med. Chem.* 47:133–142.
5. Chen, R., M. R. Tilley, H. Wei, F. Zhou, F.-M. Zhou, S. Ching, N. Quan, R. L. Stephens, E. R. Hill, T. Nottoli, D. D. Han, and H. H. Gu. 2006. Abolished cocaine reward in mice with a cocaine-insensitive dopamine transporter. *Proc. Natl. Acad. Sci. USA.* 103:9333–9338.
6. Sparenborg, S., F. Vocci, and S. Zukin. 1997. Peripheral cocaine-blocking agents: new medications for cocaine dependence. *Drug Alcohol Depend.* 48:149–151.
7. Gorelick, D. A. 1997. Enhancing cocaine metabolism with butyrylcholinesterase as a treatment strategy. *Drug Alcohol Depend.* 48: 159–165.
8. Redish, A. D. 2004. Addiction as a computational process gone awry. *Science.* 306:1944–1947.
9. Gao, D., H. Cho, W. Yang, Y. Pan, G.-F. Yang, H.-H. Tai, and C.-G. Zhan. 2006. Computational design of a human butyrylcholinesterase mutant for accelerating cocaine hydrolysis based on the transition-state simulation. *Angew. Chem. Int. Ed. Engl.* 45:653–657.
10. Gao, D., and C.-G. Zhan. 2006. Modeling evolution of hydrogen bonding and stabilization of transition states in the process of cocaine hydrolysis catalyzed by human butyrylcholinesterase. *Proteins.* 62: 99–110.
11. Pan, Y., D. Gao, W. Yang, H. Cho, G.-F. Yang, H.-H. Tai, and C.-G. Zhan. 2005. Computational redesign of human butyrylcholinesterase for anti-cocaine medication. *Proc. Natl. Acad. Sci. USA.* 102:16656–16661.
12. Zhan, C.-G., and D. Gao. 2005. Catalytic mechanism and energy barriers for butyrylcholinesterase-catalyzed hydrolysis of cocaine. *Biophys. J.* 89:3863–3872.
13. Gao, D., and C.-G. Zhan. 2005. Modeling effects of oxyanion hole on the ester hydrolyses catalyzed by human cholinesterases. *J. Phys. Chem. B.* 109:23070–23076.
14. Gaintdinov, R. R., T. D. Sotmikova, and M. G. Caron. 2002. Monoamine transporter pharmacology and mutant mice. *Trends Pharmacol. Sci.* 23:367–373.
15. Torres, G. E., R. R. Gainetdinov, and M. G. Caron. 2003. Plasma membrane monoamine transporters: structure, regulation and function. *Nat. Rev. Neurosci.* 4:13–25.
16. Chen, N., and M. E. A. Reith. 2003. Na^+ and the substrate permeation pathway in dopamine transporters. *Eur. J. Pharmacol.* 479:213–221.
17. Berfield, L. J., C. L. Wang, and E. A. M. Reith. 1999. Which form of dopamine is the substrate for the human dopamine transporter: the cationic or the uncharged species? *J. Biol. Chem.* 274:4876–4882.
18. Kitayama, S., S. Shimada, H. Xu, L. Markham, M. D. Donovan, and R. G. Uhl. 1992. Dopamine transporter site-directed mutations differentially alter substrate transport and cocaine binding. *Proc. Natl. Acad. Sci. USA.* 89:7782–7785.

19. Uhl, G. R., and Z. Lin. 2003. The top 20 dopamine transporter mutants: structure-function relationships and cocaine actions. *Eur. J. Pharmacol.* 479:71–82.

20. Loland, C. J., K. Norgaard-Nielsen, and U. Gether. 2003. Probing dopamine transporter structure and function by Zn^{2+}-site engineering. *Eur. J. Pharmacol.* 479:187–197.

21. Gu, H. H., and X. Wu. 2003. Cocaine affinity decreased by mutations of aromatic residue phenylalanine 105 in the transmembrane domain 2 of dopamine transporter. *Mol. Pharmacol.* 63:653–658.

22. Chen, N., J. Zhen, and M. E. A. Reith. 2004. Mutation of Trp^{84} and Asp^{313} of the dopamine transporter reveals similar mode of binding interaction for GBR12909 and benztropine as opposed to cocaine. *J. Neurochem.* 89:853–864.

23. Sen, N., L. Shi, T. Beuming, H. Weinstein, and J. A. Javitch. 2005. A pincer-like configuration of TM2 in the human dopamine transporter is responsible for indirect effects on cocaine binding. *Neuropharmacology.* 49:780–790.

24. Ukairo, O. T., C. D. Bondi, A. H. Neuwman, S. S. Kulkarni, A. P. Kozikowski, S. Pan, and C. K. Surratt. 2005. Recognition of benztropine by the dopamine transporter (DAT) differs from that of the classical dopamine uptake inhibitors cocaine, methylphenidate, and mazindol as a function of a DAT transmembrane 1 aspartic acid residue. *J. Pharmacol. Exp. Ther.* 314:575–583.

25. Chen, R., D. D. Han, and H. H. Gu. 2005. A triple mutation in the second transmembrane domain of mouse dopamine transporter markedly decreases sensitivity to cocaine and methylphenidate. *J. Neurochem.* 94:352–359.

26. Vaughan, R. A., D. S. Sakrikar, M. L. Parnas, S. Adkins, J. D. Foster, R. A. Duval, J. R. Lever, S. S. Kulkarni, and A. Hauck-Newman. 2007. Localization of cocaine analog [125I]RTI82 irreversible binding to transmembrane domain 6 of the dopamine transporter. *J. Biol. Chem.* 282:8915–8925.

27. Kniazeff, J., C. J. Loland, N. Goldberg, M. Quick, S. Das, H. H. Sitte, J. A. Javitch, and U. Gether. 2005. Intramolecular cross-linking in a bacterial homolog of mammalian SLC6 neurotransmitter transporters suggests an evolutionary conserved role of transmembrane segments 7 and 8. *Neuropharmacology.* 49:715–723.

28. Dar, D. E., T. G. Metzger, D. J. Vandenbergh, and G. R. Uhl. 2006. Dopamine uptake and cocaine binding mechanisms: the involvement of charged amino acids from transmembrane domains of the human dopamine transporter. *Eur. J. Pharmacol.* 538:43–47.

29. Boudker, O., R. M. Ryan, D. Yernool, K. Shimamoto, and E. Gouaux. 2007. Coupling substrate and ion binding to extracellular gate of a sodium-dependent aspartate transporter. *Nature.* 445:387–393.

30. Huang, Y., M. J. Lemieux, J. Song, M. Auer, and D.-N. Wang. 2003. Structure and mechanism of the glycerol-3-phosphate transporter from *Escherichia coli*. *Science.* 301:616–620.

31. Abramson, J., I. Smirnova, V. Kasho, G. Verner, H. R. Kaback, and S. Iwata. 2003. Structure and mechanism of the lactose permease of *Escherichia coli*. *Science.* 301:610–615.

32. Yernool, D., O. Boudker, Y. Jin, and E. Gouaux. 2004. Structure of a glutamate transporter homologue from *Pyrococcus horikoshii*. *Nature.* 431:811–818.

33. Hunte, C., E. Screpant, M. Venturi, A. Rimon, E. Padan, and H. Michel. 2005. Structure of a Na^+/H^+ antiporter and insights into mechanism of action and regulation by pH. *Nature.* 435:1197–1202.

34. Yamashita, A., S. K. Singh, T. Kawate, Y. Jin, and E. Gouaux. 2005. Crystal structure of a bacterial homologue of Na^+/Cl^--dependent neurotransmitter transporters. *Nature.* 437:215–223.

35. Ravna, A. W., I. Sylte, and S. G. Dahl. 2003. Molecular model of the neural dopamine transporter. *J. Comput. Aided Mol. Des.* 17: 367–382.

36. Ravna, A. W., I. Sylte, K. Kristiansen, and S. G. Dahl. 2006. Putative drug binding conformations of monoamine transporters. *Bioorg. Med. Chem.* 14:666–675.

37. Thompson, J. D., D. G. Higgins, and T. J. Gibson. 1994. CLUSTAL W: improving the sensitivity of progressive multiple sequence alignment through sequence weighting, position-specific gap penalties, and weight matrix choice. *Nucleic Acids Res.* 22:4673–4680.

38. Henikoff, S., and J. G. Henikoff. 1992. Amino-acid substitution matrices from protein blocks. *Proc. Natl. Acad. Sci. USA.* 89:10915–10919.

39. Humphrey, W., A. Dalke, and K. Schulten. 1996. VMD—visual molecular dynamics. *J. Mol. Graph.* 14:33–38.

40. Frisch, M. J., G. W. Trucks, H. B. Schlegel, G. E. Scuseria, M. A. Robb, J. R. Cheeseman, Jr., J. A. Montgomery, T. Vreven, K. N. Kudin, J. C. Burant, J. M. Millam, S. S. Iyengar, J. Tomasi, V. Barone, B. Mennucci, M. Cossi, G. Scalmani, N. Rega, G. A. Petersson, H. Nakatsuji, M. Hada, M. Ehara, K. Toyota, R. Fukuda, J. Hasegawa, M. Ishida, T. Nakajima, Y. Honda, O. Kitao, H. Nakai, M. Klene, X. Li, J. E. Knox, H. P. Hratchian, J. B. Cross, C. Adamo, J. Jaramillo, R. Gomperts, R. E. Stratmann, O. Yazyev, A. J. Austin, R. Cammi, C. Pomelli, J. W. Ochterski, P. Y. Ayala, K. Morokuma, G. A. Voth, P. Salvador, J. J. Dannenberg, V. G. Zakrzewski, S. Dapprich, A. D. Daniels, M. C. Strain, O. Farkas, D. K. Malick, A. D. Rabuck, K. Raghavachari, J. B. Foresman, J. V. Ortiz, Q. Cui, A. G. Baboul, S. Clifford, J. Cioslowski, B. B. Stefanov, G. Liu, A. Liashenko, P. Piskorz, I. Komaromi, R. L. Martin, D. J. Fox, T. Keith, M. A. Al-Laham, C. Y. Peng, A. Nanayakkara, M. Challacombe, P. M. W. Gill, B. Johnson, W. Chen, M. W. Wong, C. Gonzalez, and J. A. Pople. 2003. Gaussian 03, Rev. A.1. Gaussian, Pittsburgh, PA.

41. Zhan, C.-G., O. Norberto de Souza, R. Rittenhouse, and R. L. Ornstein. 1999. Determination of two structural forms of catalytic bridging ligand in zinc-phosphotriesterase by molecular dynamics simulation and quantum chemical calculation. *J. Am. Chem. Soc.* 121:7279–7282.

42. Koca, J., C.-G. Zhan, R. Rittenhouse, and R. L. Ornstein. 2001. Mobility of the active site bound paraoxon and sarin in zinc-phosphotriesterase by molecular dynamics simulation and quantum chemical calculation. *J. Am. Chem. Soc.* 123:817–826.

43. Zhan, C.-G., F. Zheng, and D. W. Landry. 2003. Fundamental reaction mechanism for cocaine hydrolysis in human butyrylcholinesterase. *J. Am. Chem. Soc.* 125:2462–2474.

44. Hamza, A., H. Cho, H.-H. Tai, and C.-G. Zhan. 2005. Understanding human 15-hydroxyprostaglandin dehydrogenase binding with NAD^+ and PGE2 by homology modeling, docking and molecular dynamics simulation. *Bioorg. Med. Chem.* 109:4776–4782.

45. Huang, X., W. Yan, D. Gao, M. Tong, H.-H. Tai, and C.-G. Zhan. 2006. Structural and functional characterization of human microsomal prostaglandin E synthase-1 (mPGES-1) by computational modeling and site-directed mutagenesis. *Bioorg. Med. Chem.* 14:3553–3562.

46. Case, D. A., T. A. Darden, T. E. Cheatham III, C. L. Simmerling, J. Wang, R. E. Duke, R. Luo, K. M. Merz, B. Wang, D. A. Pearlman, M. Crowley, S. Brozell, V. Tsui, H. Gohlke, J. Mongan, V. Hornak, G. Cui, P. Beroza, C. Schafmeister, J. W. Caldwell, W. S. Ross, and P. A. Kollman. 2004. AMBER 8. University of California, San Francisco.

47. Jorgensen, W. L., J. Chandrasekhar, J. D. Madura, and R. W. Impey. 1983. Comparison of simple potential functions for simulating liquid water. *J. Chem. Phys.* 79:926–935.

48. Morris, G. M., D. S. Goodsell, R. S. Halliday, R. Huey, W. E. Hart, R. K. Belew, and A. J. Olson. 1998. Automated docking using a Lamarckian genetic algorithm and empirical binding free energy function. *J. Comput. Chem.* 19:1639–1662.

49. Kuntz, I. D., D. T. Moustakas, and P. T. Lang. 2006. DOCK 5.4. University of California, San Francisco.

50. Solis, F. J., and R. J. B. Wets. 1981. Minimization by random search techniques. *Math. Oper. Res.* 6:19–30.

51. Kollman, P. A., I. Massova, C. Reyes, B. Kuhn, S. Huo, L. Chong, M. Lee, T. Lee, Y. Duan, W. Wang, O. Donini, P. Cieplak, J. Srinivasan, D. A. Case, and T. E. I. I. I. Cheatham. 2000. Calculating structures and free energies of complex molecules: combining molecular mechanics and continuum models. *Acc. Chem. Res.* 33:889–897.

52. Gilson, M. K., and B. Honig. 1988. Calculation of the total electrostatic energy of a macromolecular system: solvation energies, binding energies and conformational analysis. *Proteins.* 4:7–18.

53. Nicholls, A., and B. Honig. 1991. A rapid finite difference algorithm, utilizing successive over-relaxation to solve the Poisson-Boltzmann equation. *J. Comput. Chem.* 12:435–445.

54. McQuarrie, D. A. A. 1976. Statistical Mechanics. Harper & Row, New York.

55. Brooks, B. R., D. Janežič, and M. Karplus. 1995. Harmonic analysis of large systems. I. Methodology. *J. Comput. Chem.* 16:1522–1542.

56. Berendsen, H. J. C., J. P. M. Postma, W. F. van Gunsteren, A. DiNola, and J. R. Haak. 1984. Molecular dynamics with coupling to an external bath. *J. Chem. Phys.* 81:3684–3690.

57. Morishita, T. 2000. Fluctuation formulas in molecular dynamics simulations with the weak coupling heat bath. *J. Chem. Phys.* 113:2976–2982.

58. Darden, T., D. York, and L. Pedersen. 1993. Particle mesh Ewald—an $N\cdot\log(N)$ method for Ewald sums in large systems. *J. Chem. Phys.* 98:10089–10092.

59. Toukmaji, A., C. Sagui, J. Board, and T. Darden. 2000. Efficient particle-mesh Ewald based approach to fixed and induced dipolar interactions. *J. Chem. Phys.* 113:10913–10927.

60. Ryckaert, J. P., G. Ciccotti, and H. J. C. Berendsen. 1977. Numerical integration of the Cartesian equations of motion of a system with constraints: molecular dynamics of *n*-alkanes. *J. Comput. Phys.* 23:327–341.

61. Androutsellis-Theotokis, A., R. N. Goldberg, K. Ueda, T. Beppu, L. M. Beckman, L. Das, A. J. Javitch, and G. Rudnick. 2003. Characterization of a functional bacterial homologue of sodium-dependent neurotransmitter transporters. *J. Biol. Chem.* 278:12703–12709.

62. Hastrup, H., N. Sen, and A. J. Javitch. 2003. The human dopamine transporter forms a tetramer in the plasma membrane. *J. Biol. Chem.* 278:45045–45048.

63. Sitte, H. H., and M. Freissmuth. 2003. Oligomer formation by Na^+-Cl^- coupled neurotransmitter transporters. *Eur. J. Pharmacol.* 479:229–236.

64. Patargias, G., P. J. Bond, S. S. Deol, and M. S. Sansom. 2005. Molecular dynamics simulations of GlpF in a micelle versus in a bilayer: conformational dynamics of a membrane protein as a function of environment. *J. Phys. Chem. B.* 109:575–582.

65. Bismuth, Y., M. P. Kavanaugh, and B. I. Kanner. 1997. Tyrosine 140 of the γ-aminobutyric acid transporter GAT-1 plays a critical role in neurotransmitter recognition. *J. Biol. Chem.* 272:16096–16102.

66. Chen, J. G., A. Sachpatzids, and G. Rudnick. 1997. The third transmembrane domain of the serotonin transporter contains residues associated with substrate and cocaine binding. *J. Biol. Chem.* 272: 28321–28327.

67. Ponce, J., B. Biton, J. Benavides, P. Avenet, and C. Aragon. 2000. Transmembrane domain III plays an important role in ion binding and permeation in the glycine transporter GLYT2. *J. Biol. Chem.* 275: 13856–13862.

68. Rafi, B. S., Q. Cui, K. Song, X. Cheng, J. P. Tonge, and C. Simmering. 2006. Insight through molecular mechanics Poisson-Boltzmann surface area calculations into the binding affinity of triclosan and three analogues for Fab1, the *E. coli* enoyl reductase. *J. Med. Chem.* 49:4574–4580.